

# UCLA

## UCLA Previously Published Works

### Title

Pathological effects of chronic myocardial infarction on peripheral neurons mediating cardiac neurotransmission

### Permalink

<https://escholarship.org/uc/item/4192p6nq>

### Authors

Nakamura, Keijiro  
Ajijola, Olujimi A  
Aliotta, Eric  
et al.

### Publication Date

2016-05-01

### DOI

10.1016/j.autneu.2016.05.001

Peer reviewed



Published in final edited form as:

*Auton Neurosci.* 2016 May ; 197: 34–40. doi:10.1016/j.autneu.2016.05.001.

## PATHOLOGICAL EFFECTS OF CHRONIC MYOCARDIAL INFARCTION ON PERIPHERAL NEURONS MEDIATING CARDIAC NEUROTRANSMISSION

Keihiro Nakamura<sup>\*,1</sup>, Olujimi A. Ajijola<sup>\*,1</sup>, Eric Aliotta<sup>¶</sup>, J. Andrew Armour<sup>\*</sup>, Jeffrey L. Ardell<sup>\*</sup>, and Kalyanam Shivkumar<sup>\*</sup>

<sup>\*</sup>UCLA Cardiac Arrhythmia Center and Neurocardiology Research Center of Excellence, University of California, Los Angeles, CA, USA

Department of Radiology, University of California, Los Angeles, CA, USA

### Abstract

**Objective**—To determine whether chronic myocardial infarction (MI) induces structural and neurochemical changes in neurons within afferent and efferent ganglia mediating cardiac neurotransmission.

**Methods**—Neuronal somata in i) right atrial (RAGP) and ii) ventral interventricular ganglionated plexi (VIVGP), iii) stellate ganglia (SG) and iv) T1-2 dorsal root ganglia (DRG) bilaterally derived from normal (n = 8) vs. chronic MI (n = 8) porcine subjects were studied. We examined whether the morphology and neuronal nitric oxide synthase (nNOS) expression in soma of RAGP, VIVGP, DRG and SG neurons were altered as a consequence of chronic MI. In DRG, we also examined immunoreactivity of calcitonin gene related peptide (CGRP), a marker of afferent neurons.

**Results**—Chronic MI increased neuronal size and nNOS immunoreactivity in VIVGP (but not RAGP), as well as in the SG bilaterally. Across these ganglia, the increase in neuronal size was more pronounced in nNOS immunoreactive neurons. In the DRG, chronic MI also caused neuronal enlargement, and increased CGRP immunoreactivity. Further, DRG neurons expressing both nNOS and CGRP were increased in MI animals compared to controls, and represented a shift from double negative neurons.

**Conclusions**—Chronic MI impacts diverse elements within the peripheral cardiac neuraxis. That chronic MI imposes such widespread, diverse remodeling of the peripheral cardiac neuraxis must be taken into consideration when contemplating neuronal regulation of the ischemic heart.

---

Address for correspondence: Olujimi Ajijola MD PhD, UCLA Cardiac Arrhythmia Center, UCLA Health System, David Geffen School of Medicine at UCLA, Suite 660, Westwood Blvd, Los Angeles CA 90095-1679, Phone: 310 206 6433, Fax: 310 794 6492, oajijola@mednet.ucla.edu.

<sup>¶</sup>These authors contributed equally

**Publisher's Disclaimer:** This is a PDF file of an unedited manuscript that has been accepted for publication. As a service to our customers we are providing this early version of the manuscript. The manuscript will undergo copyediting, typesetting, and review of the resulting proof before it is published in its final citable form. Please note that during the production process errors may be discovered which could affect the content, and all legal disclaimers that apply to the journal pertain.

**Disclosures:** None

## Keywords

autonomic nervous system; CGRP; chronic myocardial infarction; dorsal root ganglia; intrinsic cardiac nervous system; nNOS; stellate ganglion

---

## 1. INTRODUCTION

Sudden cardiac death (SCD) due to ventricular arrhythmias (VAs) is the leading cause of mortality in the developed world, resulting in an estimated four to five million deaths each year (Chugh et al., 2008). Autonomic neuronal dysfunction plays a crucial role in the genesis of cardiac arrhythmias and/or progression of the failing heart (Fukuda et al., 2015; Vaseghi et al., 2008). The cardiac neuronal hierarchy is primarily focused on dynamic coordination of cardiac function to match whole body metabolic demands (Armour et al., 2004a) and includes neural networks located from the level of the heart (Ardell, 1994; Armour, 1991) and intra-thoracic extra-cardiac ganglia to the insular cortex (Oppenheimer et al., 1994).

At the organ level, the intrinsic cardiac nervous system (ICNS) comprises a distributed network of ganglia and interconnecting nerves (Ardell, 1994; Armour, 1991). Neurons within cardiac GPs interact in concert with neurons in intra-thoracic extra-cardiac (sympathetic) ganglia, nodose and dorsal root ganglia (DRG), and higher center neurons (including spinal neurons). Neurons throughout the cardiac neuraxis interact continuously to match cardiac output to whole body demands on a beat-to-beat basis (Ardell, 2004; Armour et al., 1990; Armour et al., 1988).

The ICNS contains all the neuronal elements necessary for cardiac reflex control independent of higher centers (Murphy et al., 2000), namely sensory neurons (Ardell et al., 1991; Armour et al., 1997; Cheng et al., 1997; Horackova et al., 1999; Yuan et al., 1994), adrenergic (Gebber et al., 1996; Lewis et al., 2001) and cholinergic (Gray et al., 2004a; Gray et al., 2004b) efferent postganglionic neurons, as well as interposed local circuit neurons (LCNs) (Beaumont et al., 2013a; Armour, 1991). The largest subpopulation, LCNs, accounts for the intra- and inter-ganglionic communication that occurs among neurons within the ICNS that sub-serves local information processing (Armour, 1991). Intra-thoracic extra-cardiac ganglia possess sensory and LCNs that target their sympathetic efferent postganglionic neurons therein. As such, collectively they are involved in intra-thoracic cardiocentric reflex control of cardiodynamics.

Cardiac disease, such as MI, adversely affects the myocardium (Cao et al., 2000; Vracko et al., 1991). How it affects neurons throughout the cardiac neuraxis, remains unknown – particularly with respect to how its varied thoracic components are affected (Ajijola et al., 2012; Ajijola et al., 2015). Neural remodeling within the cardiac nervous system post-MI contributes to autonomic imbalances (Kember et al., 2013) and the potential for SCD (Fukuda et al., 2015). It is known that human IC neurons undergo structural remodeling in the presence of chronic obstruction to their regional arterial blood supply (Hopkins et al., 2000b). Such neurons display enlarged somata that are replete with vacuoles, in addition to displaying degenerative changes in their dendrites and axons (Hopkins et al., 2000a). In the

porcine model, chronic ventricular infarction is accompanied by similar changes in somata of the stellate ganglia (SG) (Ajjola et al., 2015). In agreement with such histological evidence, *in vitro* intracellular studies of IC neurons derived from chronic MI animals have demonstrated enhanced neuronal excitability, altered synaptic efficacy, and adaptive reorganization of neurochemical phenotypes and neuromodulation within the intrinsic cardiac nervous system (Hardwick et al., 2014; Hardwick et al., 2008). In fact, it is becoming evident that the ICNS, as the final integrator of cardiac neuraxial control, can undergo significant reorganization – both anatomical and functional – during the evolution of chronic MI (Rajendran et al., 2016).

Thus, by histologic means, we sought to establish whether chronic (regional) left ventricular infarction remodels select neuronal elements within the peripheral cardiac neuraxis.

## 2. MATERIALS AND METHODS

Yorkshire pigs (35±15kg) of either gender with normal hearts (n = 8) and those with chronic left antero-apical infarctions (n = 8) were studied. All experiments were performed in accordance with the National Institute of Health *Guide for the Care and Use of Laboratory Animals* and approved by the University of California - Los Angeles Chancellor's Animal Research Committee.

### 2.1 Creation of chronic myocardial infarction

Pigs were sedated with telazol (8 mg/kg, intramuscular (IM)), intubated and then ventilated. General endotracheal anesthesia (isoflurane 1–2%, inhalation) was instituted. A 6-lead electrocardiogram (ECG) and right femoral arterial pressure were monitored. An 8-French sheath was placed in the left or right femoral artery and an Amplatz-type catheter was guided over a wire into the left main coronary artery under fluoroscopy. Using an over-the-wire technique, an angioplasty balloon catheter (3mm, Abbot Vascular, FoxCross PTA Catheter, Temecula, CA, USA) was then advanced and inflated in the mid-left anterior coronary descending (LAD) artery. Thirty seconds after balloon inflation, a five mL suspension of saline containing one mL polystyrene microspheres (Polybead 90 µm diameter, Polysciences Inc., Warrington, PA, USA) was injected distally into that artery. The MI was confirmed by the presence of ST-segment elevations in lead II of the ECG. Following this, sedation was gradually weaned, and animals extubated. Close monitoring for arrhythmias was performed for two hours after extubation, and ventricular arrhythmias treated with esmolol (5mg boluses) and lidocaine (10–20mg boluses). Following full recovery (i.e. the animal is upright and clinically stable), the animal was returned to its pen and monitored daily.

### 2.2 Characterization of chronic myocardial infarction

Cardiac magnetic resonance imaging (MRI) was performed using a 3 Tesla scanner (Magnetom Trio, A Tim System, Siemens, Munich, Germany) to confirm the location and extent of scar tissue (Figure 1A & B)(Nakahara et al., 2011). Fifteen minutes after injecting the contrast agent gadopentetate dimeglumine (0.2 mm/kg, IV; Magnevist, Bayer, Whippany, NJ, USA), animals were humanely euthanized and their hearts excised. Thereafter, cardiac

MRI images were acquired using a three-dimensional T1-weighted gradient echo sequence. A series of parallel short axis images of the entire heart were then acquired (bandwidth: 200 Hz/pixel; spatial resolution:  $0.33 \times 0.33 \times 0.50$  mm). Areas that showed hyper enhancement were considered to represent scar tissue. A left ventricular mask was first generated by manually cropping the atria and the right ventricle using Osirix image processing software (Pixmeo, Geneva, Switzerland) and applying a threshold based mask to remove background. An infarct mask was quantified by voxels with signal intensities greater than 6 standard deviations above the mean signal in the remote myocardium (as measured in a user-defined ROI). LV and infarct volumes were calculated by multiplying the number of voxels in the respective masks by the image voxel volume.

### 2.3 Terminal Study

Chronic MI animals, studied six weeks post-MI, and age-matched control animals were sedated with telazol (8 mg/kg, IM), intubated and ventilated as described above. General endotracheal anesthesia was maintained with isoflurane (1–2%, INH). Depth of anesthesia was determined by monitoring hemodynamic indices, jaw tone and pedal withdrawal reflex; anesthesia was adjusted as necessary. Right femoral venous access was obtained for fluid replacement and the right femoral artery was access for monitoring arterial pressure. Body temperature was monitored continuously and maintained via heating pads. Acid-base status was evaluated hourly; respiratory rate and tidal volume were adjusted and bicarbonate was infused as necessary to maintain blood gas homeostasis. The following tissues were collected: bilateral stellate ganglia, ventral inter-ventricular and right atrial ganglionated plexi, and bilateral dorsal root ganglia at the first-second thoracic level (T1-T2). At the completion of the tissue collection, animals were euthanized under deep anesthesia using sodium pentobarbital (100 mg/kg, IV).

### 2.4 Histological and Immunohistochemical analyses

**2.4.1 Tissue fixation**—Under general anesthesia, tissues were dissected and rapidly excised, rinsed in cold saline for 1–2 seconds, and transferred immediately to cooled phosphate-buffered formalin (10%, Fisher, Pittsburgh, PA, USA) for 3–4 days. Afterwards, tissues were rinsed in cooled saline for 1–2 seconds and transferred to cold 70% ethanol for paraffin embedding. Sections cut four 4 microns thick were placed on charged slides.

**2.4.2 Histology and immunohistochemistry**—Hematoxylin and eosin staining was used to characterize neuronal morphology, and distribution. Adrenergic neurons were identified using anti-tyrosine hydroxylase antibody (1:2000 dilution, #ab112, Abcam, Cambridge, MA, USA). nNOS immunoreactivity was detected using anti-NOS1 (1:500, sc648, Santa Cruz Biotechnology, Dallas, TX, USA). CGRP immunoreactivity was assessed using anti-CGRP (1:500, ab36001, Abcam). Prior to immunohistochemistry, slides with paraffin sections were placed in xylene to remove paraffin, and washed with ethanol. Antigen retrieval was performed by incubation for 10 minutes in EDTA Solution pH 8 for TH and nNOS (Invitrogen Corporation, Ref# 005501) at 95°C; and in Citrate solution pH 6 for CGRP using a steamer. Incubation with primary antibody was performed for one hour, and 30 minutes for secondary antibody incubation. Detection was performed using

diaminobenzidine (Life Technologies, Green Island, NY, USA) at manufacturer's recommendation for all stains.

**2.4.3 Quantification**—All slides were digitally scanned at 20–40x magnification and electronically stored for analyses (Aperio Imagescope, Leica Systems, Buffalo Grove, IL, USA). Automated quantifications were done by image analysis software in a blinded fashion using Tissue Studio, Definiens Inc, Carlsbad, CA, USA). Quantitated data obtained from computerized analyses were visually inspected and verified. Incorrect morphologic analyses (<10%) were rejected and re-run. Neuronal size is reported in  $\mu\text{m}^2$ . Intensity of neuronal staining is quantified as the brown chromogen intensity (arbitrary units).

## 2.5 Statistical Analysis

All data are expressed mean $\pm$ standard deviation (SD), unless otherwise stated. Paired comparisons were performed with the Wilcoxon signed rank test. Comparisons of >2 groups were performed with the analysis of variance (ANOVA), and post hoc comparisons with the Tukey-Kramer. Data were analyzed using Systat (Systat Software Inc., San Jose, CA, USA).

## 3. RESULTS

### 3.1 Anatomic location of chronic ventricular infarction

The zones of infarcted ventricular tissues infarcted were located in the anteroapical left ventricle and distal right ventricle. Figure 1 (A–C) depicts a representative case illustrating the location of the catheter placement in the LAD, as represented by the course of dye injected into the origin of the LAD coronary artery, to illustrate the nature of the distal left coronary arterial branches of this animal into which the microspheres were injected. The lower panels depict i) the ventral surface of a 3-D reconstructed heart derived from the terminal experiments (1D), and ii) axial and coronal magnetic resonance slices (1D–E, respectively) through the heart. The infarcted regions are shown as the pale and white regions (Figure 1D–E). Ischemic tissues, so depicted, spared the base of the ventricles where the VIVGP is located. To quantify the size of the infarct, the volume of surviving (uninfarcted) left ventricular myocardium, and infarcted scar tissue were quantified as described (Figure 1G). Mean volume of LV tissue was  $112.5\pm 15\text{ml}$ , while mean infarct volume was  $19.7\pm 5.6\text{ml}$  (Figure 1H). Across the animals studied, mean percent infarction by volume was  $17.6\pm 4.5\%$  of left ventricular volume.

### 3.2 Chronic ventricular infarction modifies the size and nNOS immunoreactivity of intrinsic cardiac neurons

When comparing the morphologic profiles of RAGP and VIVGP neurons, somata derived from VIVGP in infarcted ventricles were enlarged compared to controls ( $1008\pm 73\mu\text{m}^2$  vs.  $875\pm 54\mu\text{m}^2$ ,  $p<0.001$ ), while RAGP neurons did not show a significant difference between MI and control subjects ( $860\pm 147\mu\text{m}^2$  vs.  $838\pm 97\mu\text{m}^2$ ,  $p=0.45$ ) (Fig. 2A). Neurons in the VIVGP were differentially targeted by MI, in that almost 50% of VIVGP neurons in MI animals displayed nNOS immunoreactivity (compared to 13.8% in controls,  $p<0.001$ ) while RAGP neurons were unaffected (Fig. 2B), with only 12.7% of their neurons from MI subjects expressing nNOS ( $p<0.001$  compared to VIVGP from MI subjects). When nNOS

immunoreactivity was examined in the context of infarction-induced morphologic changes, somatal enlargement seen in VIVGP of MI subjects was driven primarily by nNOS positive neurons. The degree of enlargement was almost two-fold greater in nNOS positive vs. nNOS negative neurons (19% vs. 11%). Comparing the populations of neurons in the RAGP and VIVGP, nNOS-expressing neurons had greater diameters than nNOS negative neurons ( $p < 0.001$  for MI and Controls, and for RAGP and VIVGP). These data suggest an association between nNOS immunoreactivity and morphological changes following MI.

### 3.3 Dorsal root ganglion afferent neuronal remodeling in chronic myocardial infarction

Unlike the ICNS, neurons in the T1-T2 DRG of MI subjects did not show significant dimensional changes (Figure 3A). Mean size of these DRG neurons was  $1414 \pm 435 \mu\text{m}^2$  and  $1487 \pm 319 \mu\text{m}^2$  ( $p = 0.39$ ) when comparing controls and chronic MI animals respectively. Although MI did not significantly impact the morphology of DRG neurons, it significantly impacted the neurochemical properties of these neurons.

The fraction of neurons expressing CGRP, and nNOS were increased in chronic MI animals compared to controls ( $86.7 \pm 2.2\%$  vs  $64 \pm 4.4$ ;  $p < 0.001$  for CGRP; and  $77.1 \pm 2.0\%$  vs.  $52.5 \pm 5.2\%$ ;  $p < 0.001$  for nNOS), as shown in Figure 3B. Not only was there an increase in the fraction of neurons expressing CGRP and nNOS, the intensity of expression (measured as intensity of brown chromogen staining in arbitrary units, Figure 3E), was greater in MI animals with respect to both CGRP ( $0.70 \pm 0.03$  vs.  $0.58 \pm 0.04$ ;  $p = 0.037$ ) and nNOS ( $0.77 \pm 0.08$  vs.  $0.51 \pm 0.06$ ;  $p = 0.017$ ). Interestingly, neuronal somata assessed for labeling of both CGRP and nNOS demonstrated that MI impacted the population of neurons showing no immunoreactivity to CGRP and nNOS, presumably inducing expression of both neurochemicals. Rather than loss of neurons, this change was due to altered expression as neuronal counts in both animal groups did not differ significantly ( $238 \pm 122$  and  $165 \pm 49$  for MI and control respectively;  $p = 0.11$ ).

When morphological profiles were classified according to neurochemical phenotype, no statistically significant difference was identified when comparing nNOS positive or negative neurons, both in control and MI animals. However, MI significantly impacted the morphology of CGRP neurons. While no difference was seen in size of CGRP negative neurons among MI and controls ( $1403 \pm 69 \mu\text{m}^2$  vs.  $1311 \pm 81 \mu\text{m}^2$ ;  $p = 0.32$ ), CGRP positive neurons in DRGs were significantly larger in MI than in control animals ( $1696 \pm 82 \mu\text{m}^2$  vs.  $1419 \pm 63 \mu\text{m}^2$ ;  $p = 0.02$ , Figure 3C). Similar to the ICNS, nNOS immunoreactivity was primarily associated with larger neuronal size, when compared to neurons negative for nNOS (Figure 3C).

### 3.4 Stellate ganglion neuronal remodeling post-myocardial infarction

Chronic MI did not significantly increase the size of neuronal somata in stellate ganglia when compared to controls (respectively,  $542 \pm 21 \mu\text{m}^2$  vs  $496 \pm 11 \mu\text{m}^2$ ;  $p = 0.09$ ). However, when examined comparing left and right-sided ganglia, LSG neurons demonstrated significantly increased dimensions ( $554 \pm 24 \mu\text{m}^2$  vs.  $470 \pm 10 \mu\text{m}^2$ ;  $p = 0.002$ ) in chronic MI animals, while RSG neurons showed no significant differences between MI and control animals ( $538 \pm 25 \mu\text{m}^2$  vs.  $523 \pm 13 \mu\text{m}^2$ ; respectively,  $p = 0.6$ ).

Chronic MI increased nNOS expression in somata of both stellate ganglia. The percentage of neurons expressing nNOS increased significantly in the presence of pathology ( $40\pm 4\%$  vs.  $26\pm 4\%$ ;  $p=0.032$ ) as shown in Figure 4A–B. When examining the morphological profile of nNOS immunoreactive neurons, MI was found to increase the size of nNOS positive neurons significantly ( $618\pm 25\mu\text{m}^2$  vs.  $545\pm 13\mu\text{m}^2$ ;  $p=0.044$ ), on the other hand nNOS negative neurons were not significantly impacted by MI in terms of morphology.

#### 4. DISCUSSION

The present study describes the finding that during the evolution of chronic MI multiple populations of peripheral autonomic neurons are differentially targeted. Specifically, the ganglion subtending the region of the infarct (VIVGP), but not atrial ganglia (RAGP) were impacted. In addition, chronic MI also induces pathological changes in neurons removed from the heart, such as afferent neurons in DRG, as well as neurons involved in sympathetic motor control in SG. The pathological changes so induced included altered morphologic profiles (c.f., increased diameters) and significant cytoplasmic vacuolization. Furthermore, the histochemical profiles of many somata in VIVGP were impacted, particularly with respect to increasing numbers of nNOS positive somata in ganglia adjacent to, as well as distant from the infarct.

Remodeling that occurred in neuronal somata distributed in various peripheral autonomic ganglia secondary to the evolution of chronic infarction implies that multiple populations in the periphery were involved in some manner in the sensory transduction of focal MI to the higher neural centers involved in cardiac neuro-regulation. In fact, most if not all, of the pathology induced by the transduction of regional ventricular infarction by affected intrinsic cardiac neurons for instance, was confined to the ischemic zone secondary to direct effects of altered regional ventricular arterial blood supply. As such, these data imply that the sensory transduction of chronic infarction was also responsible for most of the pathological changes in both the distant afferent neuronal somata in DRG, and second order neurons in stellate ganglia.

Morphologic and neurochemical changes have been identified in neurons contained within sympathetic ganglia such as the SG (Ajjola et al., 2012; Ajjola et al., 2015; Hopkins et al., 2000b). SG possess not only sympathetic efferent postganglionic neurons, but also significant populations of local circuit neurons involved in cardiac regulation. The latter transduce myocardial ischemia from intra-thoracic extra-cardiac afferent neurons to sympathetic motor control of the heart (Armour, 1986). That functional remodeling of SG involved in such adrenergic control of cardiac indices occurs in the pathological processes elicited during the evolution of ventricular infarction presumably involved local circuit neurons therein, some of which display immunoreactivity to peptides such as CGRP (Darvesh et al., 1987). As such, this indicates the complexity of responses induced with intra-thoracic extra-cardiac sympathetic ganglia attending the evolution of chronic MI.

Supported by data obtained in canine and porcine animal models (Beaumont et al., 2013a), significant percentages of intrinsic cardiac neurons are modified by sensory inputs derived from all four chambers of the heart (Rajendran et al., 2016). As such, afferent neural signals

derived from the chronically infarcted ventricular tissues affect multiple populations of porcine IC neurons to modify the activity generated by multiple neuronal subtypes therein (Arora et al., 2003a). With respect to the pathological changes elicited with the ICNS during the weeks following a ventricular infarction, the time period studied herein represents a stable phase for autonomic adaptation, being well beyond any acute remodeling phase characterized by myocyte death and neural degeneration (Hardwick et al., 2014). Furthermore, as neuronal somata identified in the VIVGP are located ‘upstream’ from infarcted ventricular tissue (Arora et al., 2003b; Yuan et al., 1994), any anatomical evidence of neural remodeling could not be attributed to the direct effects of chronic lack of arterial blood supply.

Such data are in accord with the fact that acute ventricular MI in the porcine model can elicit sympathetic denervation of the infarcted myocardium and hyper-innervation of the border zones (Cao et al., 2000; Vracko et al., 1991). The vast majority of the neurons involved in the pathological processes herein appeared to be local circuit in nature, given the diameters of their somata (relatively large compared to other somata) and immune-reactive profiles - as correlated with normal neuronal somata previously identified (Beaumont et al., 2013b). Their pathological adaptation may represent remodeling such that the peripheral network becomes grossly destabilized due to the tonic nature of afferent neuronal inputs arising from chronic ischemic ventricular tissues that induces such neuronal remodeling.

It is known that chronic ventricular infarction induces pathological changes in autonomic neurons located in multiple nexus points within the ICNS (Rajendran et al., 2016). Local circuit neurons in each nexus point of the peripheral autonomic nervous system involved in cardiac regulation represent the major information processor of cardiac sensory information. It appears that the capacity of these populations to transduce chronic MI to cardiac motor neurons undergoes significant pathology during the evolution of MI. The pathological findings of this study further indicate that the capacity to process cardiac sensory information to convergent LCNs throughout the intrinsic cardiac nervous system, but also in intra-thoracic extra-cardiac sympathetic ganglia, remodels post-MI. Presumably, that would result in altered integrated network control in response to cardiovascular stressors.

Given the scope of the pathological evidence presented herein, the responsiveness of the peripheral components within the cardiac neuraxis to such pathology would likely elicit major reductions in function. As such, it appears that MI-induced remodeling of afferent neural signal transduced throughout the cardiac neuraxis results in direct and significant pathological changes in the very anatomical substrate that is constantly attempting to maintain adequacy of cardiac output for whole body perfusion.

## 5. LIMITATIONS, PERSPECTIVES AND SIGNIFICANCE

The present study sheds light on the global nature of the effects that ventricular afferent neurons transducing MI exert on the rest of the cardiac neuraxis. This includes pathological changes occurring not only in adjacent neurons (i.e., those in adjacent intrinsic cardiac ganglia), but those in remote such as thoracic DRGs. Since such neurons are tasked with adequacy of cardiac function, transducing chronic MI evidently elicits fundamental changes

to peripheral and central reflex control of the diseased heart. A limitation of this study is that these changes were not related to cardiac-specific neurons in the SG or DRG. In addition, we cannot directly distinguish between neural effects related to the infarct directly (i.e. myocardial injury and the process of remodeling), or to the hemodynamic insult (i.e. reduced cardiac output).

Modulation of afferent neural signals derived from the diseased myocardium to the hierarchy may represent a novel therapeutic target for mitigating ischemic heart diseases. As such, how neurons throughout the periphery remodel post-MI and how control system responds to such pathology needs to be fully explored.

## Acknowledgments

The authors wish to thank Amiksha Gandhi, and Tadanobu Irie MD for excellent technical assistance.

### 7. SOURCES OF FUNDING

This study was supported by National Institutes of Health (NIH) National Heart, Lung, and Blood Institute (NHLBI) grant HL125730 (O.A.A); HL071830 (J.L.A.); and HL084261 (K.S.).

## NON-STANDARD ABBREVIATIONS AND ACRONYMS

<b>ANS</b>	autonomic nervous system
<b>MI</b>	myocardial infarction
<b>ICNS</b>	intrinsic cardiac nervous system
<b>LCN</b>	local circuit neuron
<b>ECG</b>	electrocardiogram
<b>LAD</b>	left anterior descending coronary artery
<b>IV</b>	intravenous
<b>VIV GP</b>	ventral interventricular ganglionated plexus
<b>DRG</b>	dorsal root ganglion
<b>LV</b>	left ventricle/ventricular
<b>RVOT</b>	right ventricular outflow tract
<b>MRI</b>	magnetic resonance imaging
<b>SG</b>	stellate ganglion

## REFERENCES

Ajjjola OA, Wisco JJ, Lambert HW, Mahajan A, Stark E, Fishbein MC, Shivkumar K. Extracardiac neural remodeling in humans with cardiomyopathy. *Circ Arrhythm Electrophysiol.* 2012; 5:1010–1116. [PubMed: 22923270]

- Ajjola OA, Yagishita D, Reddy NK, Yamakawa K, Vaseghi M, Downs AM, Hoover DB, Ardell JL, Shivkumar K. Remodeling of stellate ganglion neurons after spatially targeted myocardial infarction: Neuropeptide and morphologic changes. *Heart Rhythm*. 2015; 12:1027–1035. [PubMed: 25640636]
- Ardell, J. Intrathoracic neuronal regulation of cardiac function. In: Armour, J.; Ardell, J., editors. *Basic and Clinical Neurocardiology*. New York: Oxford University Press; 2004. p. 187-219.
- Ardell, JL. *Structure and function of mammalian intrinsic cardiac neurons*. New York: Neurocardiology Oxford University Press; 1994.
- Ardell JL, Butler CK, Smith FM, Hopkins DA, Armour JA. Activity of in vivo atrial and ventricular neurons in chronically decentralized canine hearts. *Am J Physiol*. 1991; 260:H713–H721. [PubMed: 2000967]
- Armour JA. Activity of in situ stellate ganglion neurons of dogs recorded extracellularly. *Can J Physiol Pharmacol*. 1986; 64:101–111. [PubMed: 3697827]
- Armour JA. Intrinsic cardiac neurons. *J Cardiovasc Electrophysiol*. 1991; 2:10.
- Armour JA. Myocardial ischaemia and the cardiac nervous system. *Cardiovasc Res*. 1999; 41:41–54. [PubMed: 10325952]
- Armour, JA.; Ardell, JL., editors. *Basic and Clinical Neurocardiology*. New York: Oxford University Press; 2004a.
- Armour, JA.; Ardell, JL. *Basic and clinical neurocardiology* Oxford University Press. New York: Oxford, xii; 2004b. p. 463
- Armour JA, Hopkins DA. Activity of in vivo canine ventricular neurons. *Am J Physiol*. 1990; 258:H326–H336. [PubMed: 2309901]
- Armour JA, Janes RD. Neuronal activity recorded extracellularly from in situ canine mediastinal ganglia. *Can J Physiol Pharmacol*. 1988; 66:119–127. [PubMed: 3370543]
- Armour JA, Murphy DA, Yuan BX, Macdonald S, Hopkins DA. Gross and microscopic anatomy of the human intrinsic cardiac nervous system. *Anat Rec*. 1997; 247:289–298. [PubMed: 9026008]
- Arora RC, Armour JA. Adenosine A1 receptor activation reduces myocardial reperfusion effects on intrinsic cardiac nervous system. *Am J Physiol Regul Integr Comp Physiol*. 2003a; 284:R1314–R1321. [PubMed: 12676752]
- Arora RC, Waldmann M, Hopkins DA, Armour JA. Porcine intrinsic cardiac ganglia. *Anat Rec A Discov Mol Cell Evol Biol*. 2003b; 271:249–258. [PubMed: 12552641]
- Beaumont E, Salavatian S, Southerland EM, Vinet A, Jacquemet V, Armour JA, Ardell JL. Network interactions within the canine intrinsic cardiac nervous system: implications for reflex control of regional cardiac function. *J Physiol*. 2013a; 591:4515–4533. [PubMed: 23818689]
- Beaumont E, Salavatian S, Southerland EM, Vinet A, Jacquemet V, Armour JA, Ardell JL. Network interactions within the canine intrinsic cardiac nervous system: implications for reflex control of regional cardiac function. *J Physiol*. 2013b; 591:4515–4533. [PubMed: 23818689]
- Cao JM, Fishbein MC, Han JB, Lai WW, Lai AC, Wu TJ, Czer L, Wolf PL, Denton TA, Shintaku IP, Chen PS, Chen LS. Relationship between regional cardiac hyperinnervation and ventricular arrhythmia. *Circulation*. 2000; 101:1960–1969. [PubMed: 10779463]
- Cheng Z, Powley TL, Schwaber JS, Doyle FJ. Vagal afferent innervation of the atria of the rat heart reconstructed with confocal microscopy. *J Comp Neurol*. 1997; 381:1–17. [PubMed: 9087415]
- Chugh SS, Reinier K, Teodorescu C, Evanado A, Kehr E, Al Samara M, Mariani R, Gunson K, Jui J. Epidemiology of sudden cardiac death: clinical and research implications. *Progress in cardiovascular diseases*. 2008; 51:213–228. [PubMed: 19026856]
- Darvesh S, Nance DM, Hopkins DA, Armour JA. Distribution of neuropeptide-like immunoreactivity in intact and chronically decentralized middle cervical and stellate ganglia of dogs. *Journal of the autonomic nervous system*. 1987; 21:167–180. [PubMed: 2453549]
- Fukuda K, Kanazawa H, Aizawa Y, Ardell JL, Shivkumar K. Cardiac Innervation and Sudden Cardiac Death. *Circ Res*. 2015; 116:2005–2019. [PubMed: 26044253]
- Gebber GL, Zhong S, Paitel Y. Bispectral analysis of complex patterns of sympathetic nerve discharge. *Am J Physiol*. 1996; 271:R1173–R1185. [PubMed: 8945951]

- Gray AL, Johnson TA, Ardell JL, Massari VJ. Parasympathetic control of the heart. II. A novel interganglionic intrinsic cardiac circuit mediates neural control of heart rate. *Journal of applied physiology*. 2004a; 96:2273–2278. [PubMed: 14978001]
- Gray AL, Johnson TA, Lauenstein JM, Newton SS, Ardell JL, Massari VJ. Parasympathetic control of the heart. III. Neuropeptide Y-immunoreactive nerve terminals synapse on three populations of negative chronotropic vagal preganglionic neurons. *J Appl Physiol* (1985). 2004b; 96:2279–2287. [PubMed: 14978003]
- Hardwick JC, Ryan SE, Beaumont E, Ardell JL, Southerland EM. Dynamic remodeling of the guinea pig intrinsic cardiac plexus induced by chronic myocardial infarction. *Auton Neurosci*. 2014; 181:4–12. [PubMed: 24220238]
- Hardwick JC, Southerland EM, Ardell JL. Chronic myocardial infarction induces phenotypic and functional remodeling in the guinea pig cardiac plexus. *American journal of physiology. Regulatory, integrative and comparative physiology*. 2008; 295:R1926–R1933.
- Hopkins DA, Macdonald SE, Murphy DA, Armour JA. Pathology of intrinsic cardiac neurons from ischemic human hearts. *The Anatomical record*. 2000a; 259:424–436. [PubMed: 10903534]
- Hopkins DA, Macdonald SE, Murphy DA, Armour JA. Pathology of intrinsic cardiac neurons from ischemic human hearts. *Anat Rec*. 2000b; 259:424–436. [PubMed: 10903534]
- Horackova M, Armour JA, Byczko Z. Distribution of intrinsic cardiac neurons in whole-mount guinea pig atria identified by multiple neurochemical coding. A confocal microscope study. *Cell Tissue Res*. 1999; 297:409–421. [PubMed: 10460488]
- Huang MH, Horackova M, Negoescu RM, Wolf S, Armour JA. Polysensory response characteristics of dorsal root ganglion neurones that may serve sensory functions during myocardial ischaemia. *Cardiovasc Res*. 1996; 32:503–515. [PubMed: 8881511]
- Armour JA. Anatomy and function of the intrathoracic neurons regulating the mammalian heart. In: IH, Z.; JP, G., editors. *Reflex Control of the Circulation*. Boca Raton, Florida: CRC Press; 1991. p. 1-37.
- Kember G, Armour JA, Zamir M. Neural control hierarchy of the heart has not evolved to deal with myocardial ischemia. *Physiol Genomics*. 2013; 45:638–644. [PubMed: 23695889]
- Kember GC, Zamir M, Armour JA. “Smart” baroreception along the aortic arch, with reference to essential hypertension. *Phys Rev E Stat Nonlin Soft Matter Phys*. 2004; 70
- Lewis CD, Gebber GL, Larsen PD, Barman SM. Long-term correlations in the spike trains of medullary sympathetic neurons. *J Neurophysiol*. 2001; 85:1614–1622. [PubMed: 11287485]
- Malliani A, Pagani M, Pizzinelli P, Furlan R, Guzzetti S. Cardiovascular reflexes mediated by sympathetic afferent fibers. *Journal of the Autonomic Nervous System*. 1983; 7:295–301. [PubMed: 6875194]
- Murphy DA, Thompson GW, Ardell JL, McCraty R, Stevenson RS, Sangalang VE, Cardinal R, Wilkinson M, Craig S, Smith FM, Kingma JG, Armour JA. The heart reinnervates after transplantation. *The Annals of thoracic surgery*. 2000; 69:1769–1781. [PubMed: 10892922]
- Nakahara S, Vaseghi M, Ramirez RJ, Fonseca CG, Lai CK, Finn JP, Mahajan A, Boyle NG, Shivkumar K. Characterization of myocardial scars: electrophysiological imaging correlates in a porcine infarct model. *Heart Rhythm*. 2011; 8:1060–1067. [PubMed: 21354335]
- Rajendran PS, Nakamura K, Ajijola OA, Vaseghi M, Armour JA, Ardell JL, Shivkumar K. Myocardial infarction induces structural and functional remodelling of the intrinsic cardiac nervous system. *The Journal of physiology*. 2016; 594:321–341. [PubMed: 26572244]
- Oppenheimer, SM.; Hopkins, DA. Suprabulbar neuronal regulation of the heart. In: JA, A.; JL, A., editors. *Neurocardiology*. New York: Oxford University Press; 1994. p. 309-342.
- Vaseghi M, Shivkumar K. The role of the autonomic nervous system in sudden cardiac death. *Progress in cardiovascular diseases*. 2008; 50:404–419. [PubMed: 18474284]
- Vracko R, Thorning D, Frederickson RG. Nerve fibers in human myocardial scars. *Hum Pathol*. 1991; 22:138–146. [PubMed: 1705914]
- Yuan BX, Ardell JL, Hopkins DA, Losier AM, Armour JA. Gross and microscopic anatomy of the canine intrinsic cardiac nervous system. *The Anatomical record*. 1994; 239:75–87. [PubMed: 8037379]

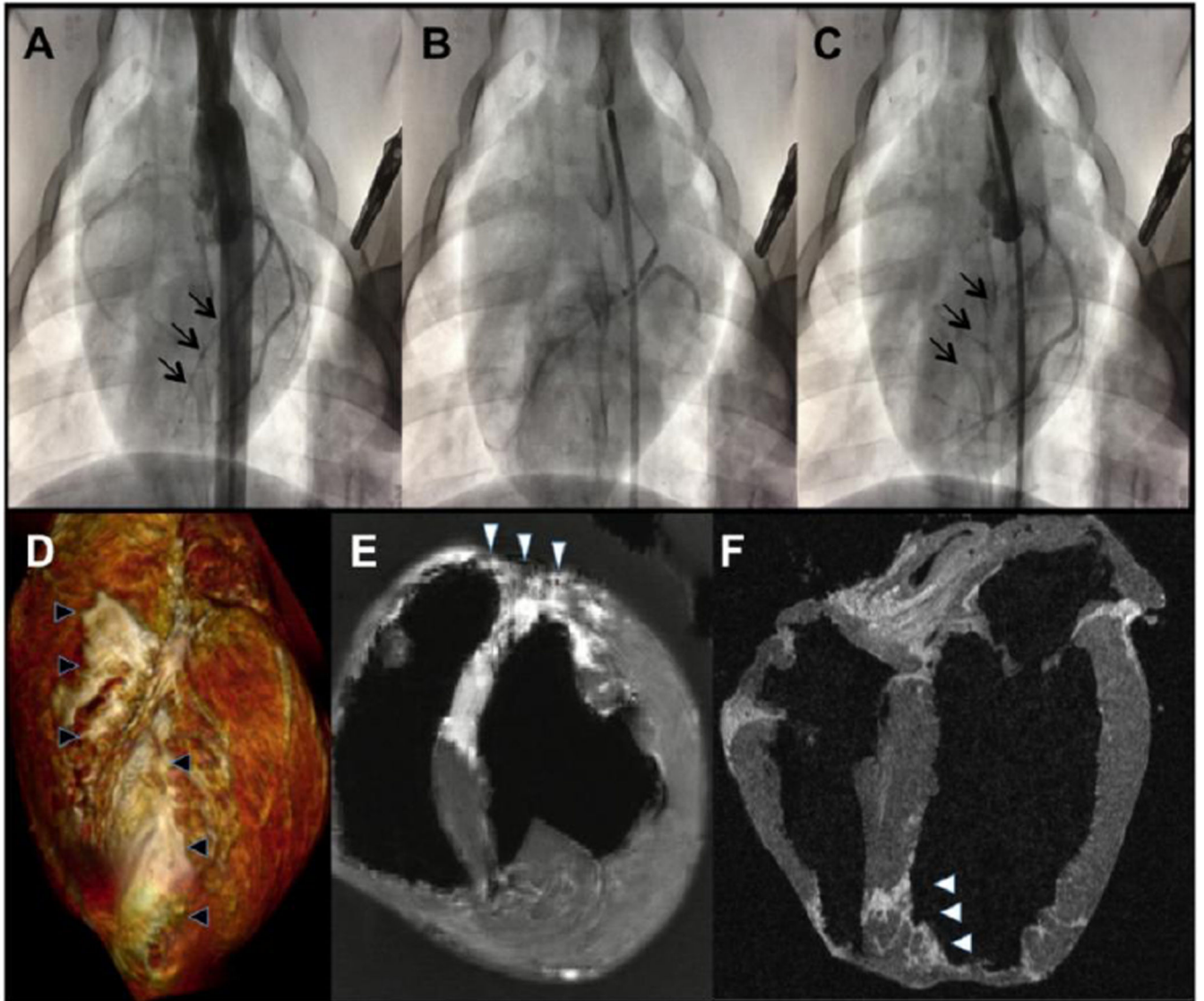


**Figure 1a**

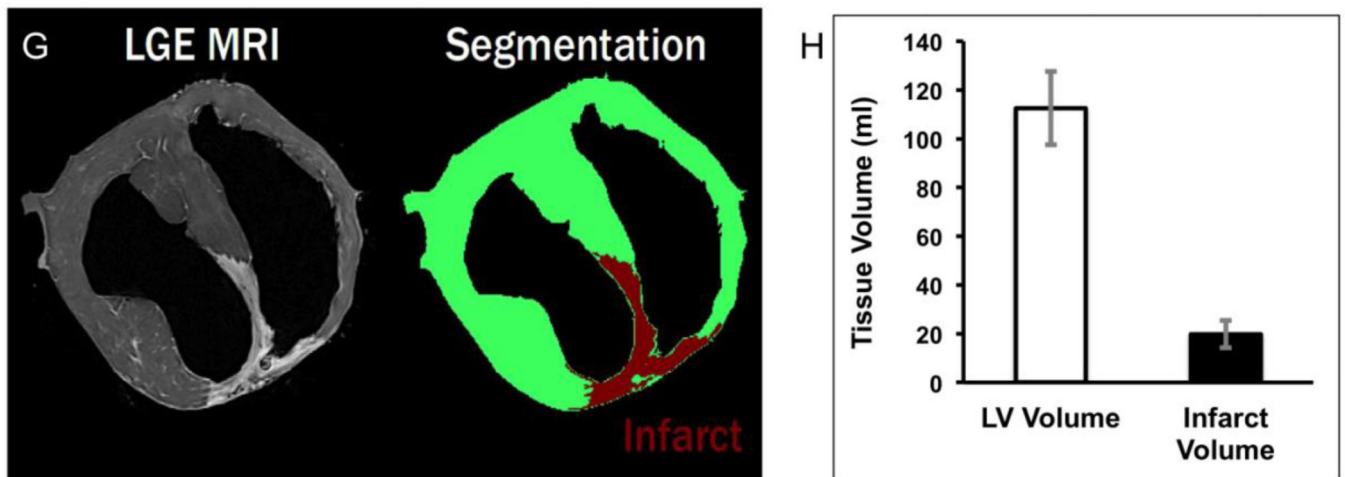


### Figure 1b

#### Figure 1. Myocardial Infarct Model

The induction and location of anteroapical myocardial infarction is shown in the upper and lower panels. The course of the left anterior descending (LAD) coronary artery is indicated by the black arrows in panel A. Injection of microspheres is shown in panel B. Following microsphere injection, absence of flow in the LAD is indicated by the black arrows in panel C. Panel D shows a 3-dimensional reconstruction of an infarcted heart, with the region of anterior infarction indicated by the black arrow heads. Panels E and F show axial and coronal contrast-enhanced magnetic resonance slices of an infarcted heart respectively, with the infarct indicated by the white arrow heads. Panels G and H show the methodology of infarct segmentation, and the quantifications of left ventricular (LV) volume and infarct volume. Data in panel H are mean $\pm$ standard deviation.

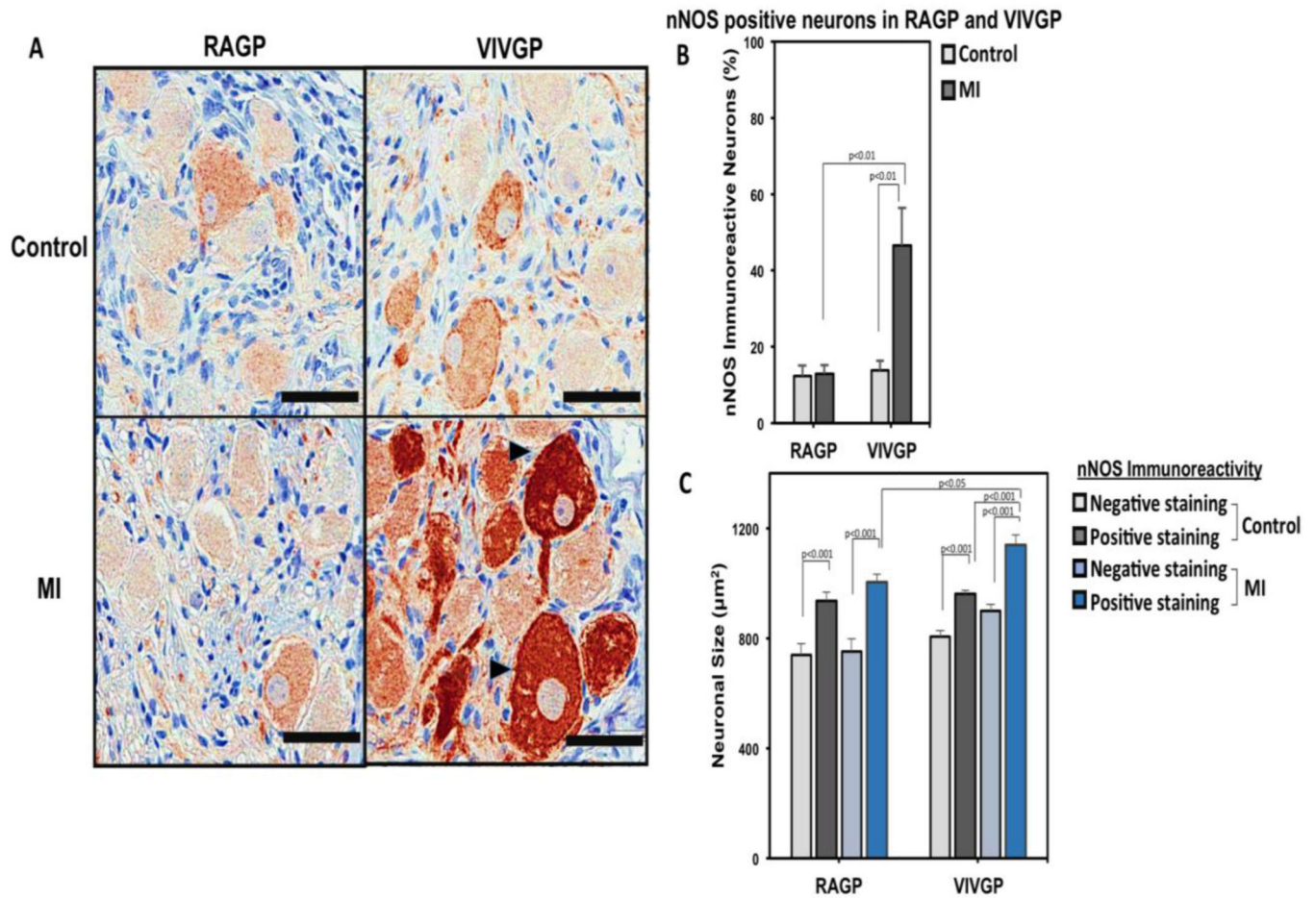


### Figure 2. Differential Neuronal Enlargement and Increases nNOS Expression in Cardiac Ganglionated Plexi

Representative immunohistochemical stains of neurons in the right atrial (RAGP) and ventral interventricular ganglionated plexi (VIVGP) are shown in panel A (scale bar: 50 µm). The larger neurons in the VIVGP can be appreciated, as well as the intensity of neuronal nitric oxide synthase (nNOS). The percentage of nNOS positive neurons in the RAGP and VIVGP are shown in panel B. The relationship between neuronal morphology and nNOS immunoreactivity for RAGP and VIVGP neurons is shown in panel C.

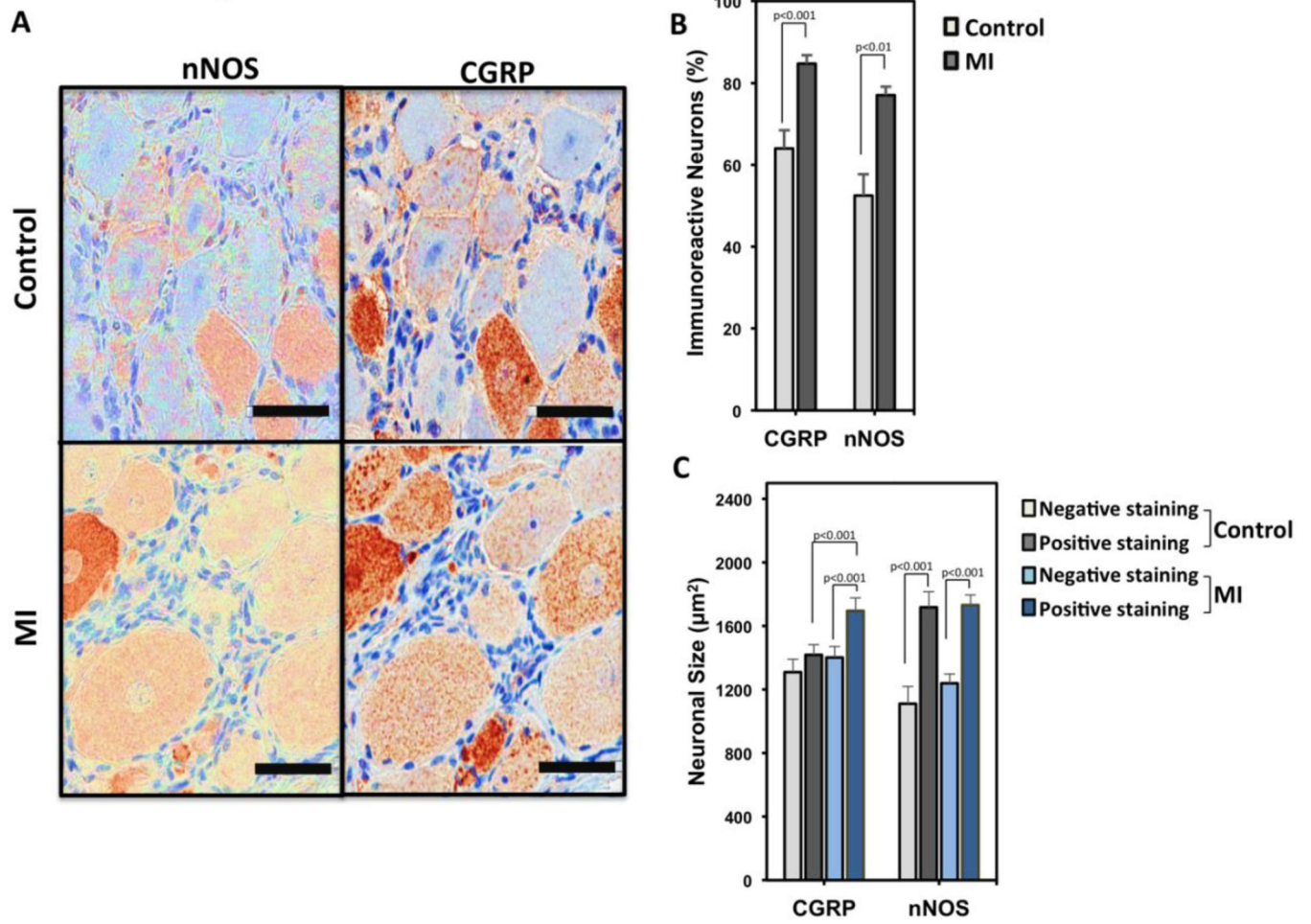
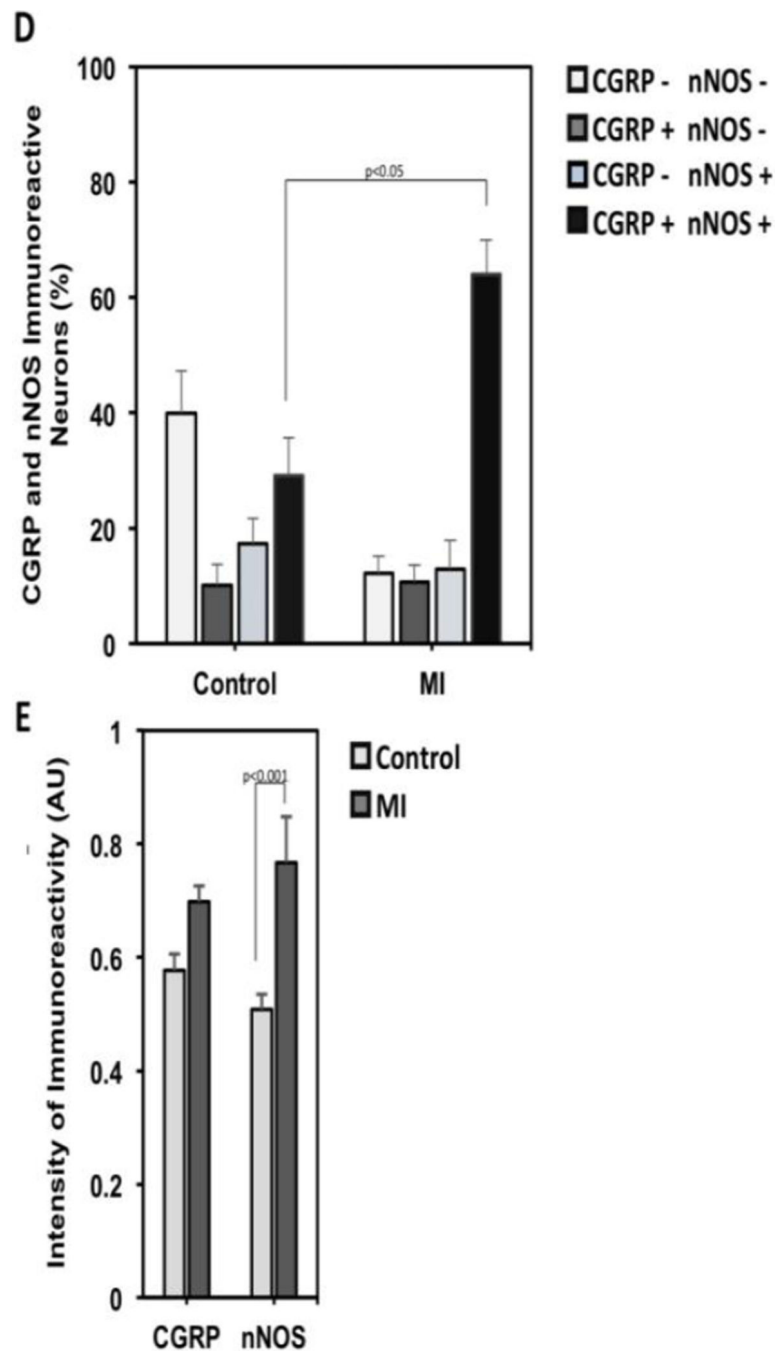


Figure 3a



**Figure 3b**

**Figure 3. Impact of chronic ischemia on morphologic and neurochemical profiles of sympathetic afferent neurons**

In Panel A, representative immunohistochemical stains of neuronal nitric oxide synthase (nNOS) and calcitonin gene related peptide (CGRP) in dorsal root ganglion (DRG) neurons is shown. The graphical quantifications of nNOS and CGRP immunoreactivity is shown in panel B. The distribution of neuronal sizes by CGRP and nNOS immunoreactivity is shown in panel C. CGRP and nNOS co-labeling in DRG neurons is shown in panel D in control and

MI states. The decrease in double negative neurons, and increase in double positive neurons can be readily appreciated. Panel E shows the the intensity of CGRP and nNOS staining in controls and MI animals (scale bar: 50  $\mu\text{m}$ ).

Author Manuscript

Author Manuscript

Author Manuscript

Author Manuscript

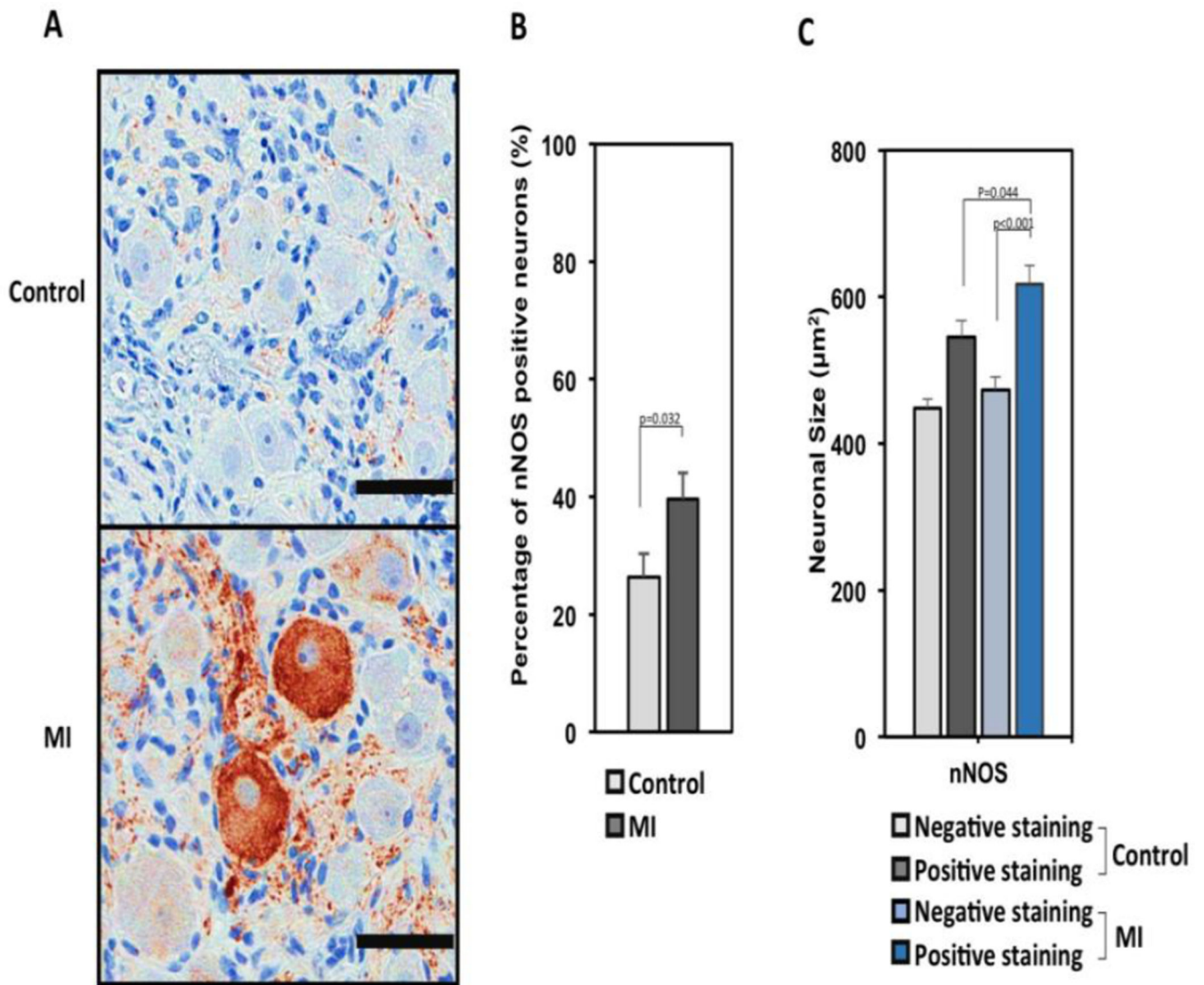


**Figure 4. Myocardial Infarction Induces Increased nNOS Expression with Neuronal Enlargement in Stellate Ganglia**

The morphologic profile and neuronal nitric oxide synthase (nNOS) immunoreactivity of left stellate ganglion (LSG) neurons are shown in panel A. The neurons can be appreciated to be larger, and nNOS immunoreactivity greater. Panels B and C show the fraction of nNOS immunoreactivity, and the distribution of neuronal sizes based on nNOS staining in stellate ganglion neurons, respectively (scale bar: 50 µm).